

## SUPPORTING INFORMATION

### Hybrid organic-inorganic connectivity of Nd<sup>III</sup>(pyrazine-N,N'-dioxide)[Co<sup>III</sup>(CN)<sub>6</sub>]<sup>3-</sup> coordination chains for creating near-infrared emissive Nd(III) showing a field-induced slow magnetic relaxation

Szymon Chorazy,<sup>\*,a</sup> Tomasz Charytanowicz,<sup>a</sup> Junhao Wang,<sup>b</sup> Shin-ichi Ohkoshi,<sup>b</sup> and Barbara Sieklucka<sup>a</sup>

<sup>a</sup>Faculty of Chemistry, Jagiellonian University, Gronostajowa 2, 30-387 Krakow, Poland.

<sup>b</sup>Department of Chemistry, School of Science, The University of Tokyo, 7-3-1 Hongo, Bunkyo-ku, Tokyo 113-0033, Japan.

\*Corresponding author: chorazy@chemia.uj.edu.pl

Experimental details.	S2
Infrared absorption spectrum of the single crystal and the polycrystalline sample of <b>1</b> . (Figure S1)	S4
Thermogravimetric curve of <b>1</b> with the related comment. (Figure S2)	S5
Crystal data and structure refinement for <b>1</b> . (Table S1)	S6
Detailed structure parameters of <b>1</b> . (Table S2)	S7
Results of Continuous Shape Measure Analysis for the nine-coordinated [Nd <sup>III</sup> (pzdo)(H <sub>2</sub> O) <sub>4</sub> (NC) <sub>3</sub> ] complex in <b>1</b> . (Table S3)	S8
Results of Continuous Shape Measure Analysis for the six-coordinated [Co <sup>III</sup> (CN) <sub>6</sub> ] <sup>3-</sup> complex in <b>1</b> . (Table S4)	S8
Asymmetric unit of <b>1</b> with the non-hydrogen atoms labelling scheme. (Figure S3)	S9
The supramolecular arrangement of cyanido-bridged chains and non-coordinated pzdo molecules of <b>1</b> with the insight into the related hydrogen bonds. (Figure S4)	S10
Detailed interatomic distances of hydrogen bonds network of <b>1</b> . (Table S5)	S10
Powder diffraction pattern of the polycrystalline sample of <b>1</b> . (Figure S5)	S11
Direct-current magnetic properties of <b>1</b> . (Figure S6)	S12
Zero-field cooled (ZFC) and field-cooled (FC) magnetic susceptibility curves of <b>1</b> . (Figure S7)	S12
Frequency dependences of in-phase $\chi_M'$ and out-of-phase $\chi_M''$ magnetic susceptibilities of <b>1</b> under <i>ac</i> magnetic field of 1 Oe, at <i>T</i> = 1.8 K and <i>T</i> = 4 K, at various values of <i>dc</i> magnetic field. (Figure S8)	S13
Parameters obtained by fitting the Argand $\chi_M''-\chi_M'$ plots of <b>1</b> for <i>H</i> <sub>dc</sub> = 1000 Oe using the generalized Debye model. (Table S6)	S14
Temperature dependence of the relaxation time of <b>1</b> for <i>H</i> <sub>dc</sub> = 1000 Oe with the results of two possible fitting procedures. (Figure S9)	S15
Overview of Nd <sup>III</sup> complexes revealing Single-Molecule Magnet behaviour. (Table S7)	S16
Solid state UV-Vis-NIR absorption (Kubelka-Munk function) spectra of <b>1</b> compared with the relevant spectra of pyrazine N,N'-dioxide and K <sub>3</sub> [Co(CN) <sub>6</sub> ]. (Figure S10)	S17
Analysis of the solid state UV-Vis-NIR absorption spectrum of <b>1</b> compared with the analyses of the relevant spectra of pyrazine N,N'-dioxide (pzdo) and K <sub>3</sub> [Co <sup>III</sup> (CN) <sub>6</sub> ]. (Table S8)	S18
Solid state excitation and emission spectra of pyrazine N,N'-dioxide collected at 77 K. (Figure S11)	S19
Solid state excitation and emission spectra of K <sub>3</sub> [Co <sup>III</sup> (CN) <sub>6</sub> ] collected at 77 K. (Figure S12)	S19
References to Supporting Information.	S20

## Experimental details.

### Materials

Neodymium(III) chloride hexahydrate ( $\text{Nd}^{\text{III}}\text{Cl}_3 \cdot 6\text{H}_2\text{O}$ , CAS: 13477-89-9, Sigma-Aldrich) and potassium hexacyanidocobaltate(III) ( $\text{K}_3[\text{Co}^{\text{III}}(\text{CN})_6]$ , CAS: 13963-58-1, Sigma-Aldrich) were purchased from commercial sources, and used without further purification. Pyrazine  $\text{N,N}'$ -dioxide (pzdo) was prepared following the published procedure through the oxidation of commercially available pyrazine (CAS: 290-37-9, Sigma-Aldrich) by using the hydrogen peroxide under heating in the acidic water solution.<sup>S1</sup> All the solvents used in the syntheses were reagent grade, purchased from commercial sources, and used without further purification.

### Synthesis and basic characterization of **1**

For the synthesis of **1**, three separate precursor solutions were prepared. Light pink solution I was obtained by dissolving the 0.4 mmol (143 mg) portion of  $\text{Nd}^{\text{III}}\text{Cl}_3 \cdot 6\text{H}_2\text{O}$  in the 10 mL of distilled water. Light yellow solution II was prepared by dissolving the 2 mmol (224 mg) portion of pzdo in the 10 mL of ethanol. Colourless solution III was obtained by dissolving the 0.4 mmol (133 mg) of  $\text{K}_3[\text{Co}^{\text{III}}(\text{CN})_6]$  in the 10 mL of distiller water. The freshly prepared solution II was added slowly to the solution I, and the resulting mixture was stirred for five minutes. Then, the solution III was slowly added, and the resulting mixture stirred for five minutes. It gave the almost colourless mixture with the small amount of white impurities which were separated by suction filtration. The clear filtrate was left closed for crystallization. After a few days, the light pink platelet crystals of **1** were collected by suction filtration, washed by ethanol, and dried on the air. The resulting crystalline material was stable on the air, and could be identified by the composition of  $\{[\text{Nd}^{\text{III}}(\text{pzdo})(\text{H}_2\text{O})_4][\text{Co}^{\text{III}}(\text{CN})_6]\} \cdot 0.5(\text{pzdo}) \cdot 4\text{H}_2\text{O}$  (**1**) as determined by the single-crystal X-ray diffraction analysis, and confirmed by the CHN elemental analysis, IR spectra (Figure S1), and thermogravimetric studies (Figure S2). Yield: 126 mg, 47%.

IR spectrum ( $\text{cm}^{-1}$ , Figure S1). Cyanides stretching vibrations: 2171m, 2160s, 2139sh, 2136s, 2128s, 2124sh, 2113w, indicated the presence of both bridging and terminal cyanides within the  $[\text{Co}^{\text{III}}(\text{CN})_6]^{3-}$  moieties.<sup>S2-S5</sup> A series of peaks in the 1500–750  $\text{cm}^{-1}$  range confirm the presence of pyrazine  $\text{N,N}'$ -dioxide.<sup>S1</sup>

CHN elemental analysis. Anal. Calcd. for  $\text{Nd}_1\text{Co}_1\text{C}_{12}\text{H}_{22}\text{N}_9\text{O}_{11}$  (**1**,  $M_{\text{W}} = 671.53 \text{ g} \cdot \text{mol}^{-1}$ ): C, 21.46%; H, 3.30%; N, 18.77%. Found: C, 21.47%, H, 3.33%; N, 18.88%.

### Crystal structure determination

Single crystal X-ray diffraction measurement for **1** was performed using a Bruker D8 Quest Eco Photon50 CMOS diffractometer equipped with Mo  $\text{K}\alpha$  radiation and a graphite monochromator. The selected well-shaped single crystal was taken from the mother solution, covered with Apiezon® N grease, and measured at the low temperature of 120(2) K (Table S1). Data reduction and cell refinement were conducted using the SAINT and SADABS programs. The reflections intensities were corrected for the compound absorption by a multi-scan method. The structure was solved by an intrinsic phasing method using a SHELXT, and refined using a weighted full-matrix least-squares technique on  $F^2$  within the SHELX-2014/7.<sup>S6-S7</sup> Further calculations were executed using a WinGX (ver. 2014.1) integrated system.<sup>S8</sup>

In the crystal structure of **1**, all non-hydrogen atoms were refined anisotropically. The hydrogen atoms were found independently from the electron density map, and refined isotropically using a riding model. The positions of most of the hydrogen atoms were restrained by using the DFIX commands for the respective O–H and C–H distances which ensure the convergence of the refinement process, and the proper geometry of the related water molecules and pzdo ligands. Structural diagrams (Figures 1 and S3–S4) were prepared using Mercury 3.5.1 software. CCDC reference number for the crystal structure of **1** is 1811806.

## Physical techniques

Infrared absorption spectra of **1** were collected on the tiny single crystals using a Nicolet iN10 MX FTIR microscope, settled in a transmission mode, and, for the comparison, on the polycrystalline sample mixed and grinded with KBr on a Jasco FTIR-4100 spectrometer. The UV-Vis-NIR diffuse reflectance spectra of **1** and the reference materials were measured on the polycrystalline samples grinded with barium sulphate using a Jasco V-670 spectrophotometer. Thermogravimetric curve was measured on a Rigaku Thermo Plus TG8120 in the 20–375 °C range under an air atmosphere under a heating rate of 1 °C·min<sup>-1</sup>. Elemental analysis of C, H, and N elements were performed using an EuroEA EuroVector elemental analyser. Powder X-ray diffraction pattern of **1** was collected for the air-dried polycrystalline sample using a PANalytical X'Pert PRO MPD diffractometer equipped with a Cu-K $\alpha$  radiation source, and a capillary system to avoid the disturbing effect of the preferred orientation of the platelet microcrystals.

Solid state photoluminescent spectra, including emission and excitation spectra, were gathered using a Horiba Jobin-Yvon Fluorolog-3 (FL3-211) spectrofluorimeter (model TKN-7) equipped with an Xe (450 W) lamp. For the UV-Vis range of 250–850 nm, a room temperature R928P emission detector operating in photon-counting mode was applied. For measurements in the NIR region of 800–1550 nm, a liquid-nitrogen-cooled version of an InGaAs photodiode detector DSS-IGA020 L was used. The emission and excitation data were collected and analysed using FluorEssence® software. Part of the measurements were performed at 77 K in a cryostat filled with liquid nitrogen.

Magnetic properties were investigated using a Quantum Design MPMS-3 Evercool magnetometer. The microcrystals covered by the small amount of the water/ethanol mixture was loaded into two plastic bags. Then, the sample was fixed to long quartz stick using small piece of a kapton tape. The data of magnetic susceptibility were corrected for the diamagnetic contributions of the sample holders (foil and kapton), and diamagnetism of the samples themselves using Pascal constants.<sup>S9</sup>

## Calculations

Continuous Shape Measure Analysis for coordination sphere of nine-coordinated Nd<sup>III</sup> and six-coordinated Co<sup>III</sup> complexes of **1** was conducted using SHAPE software ver. 2.1.<sup>S10-S11</sup>

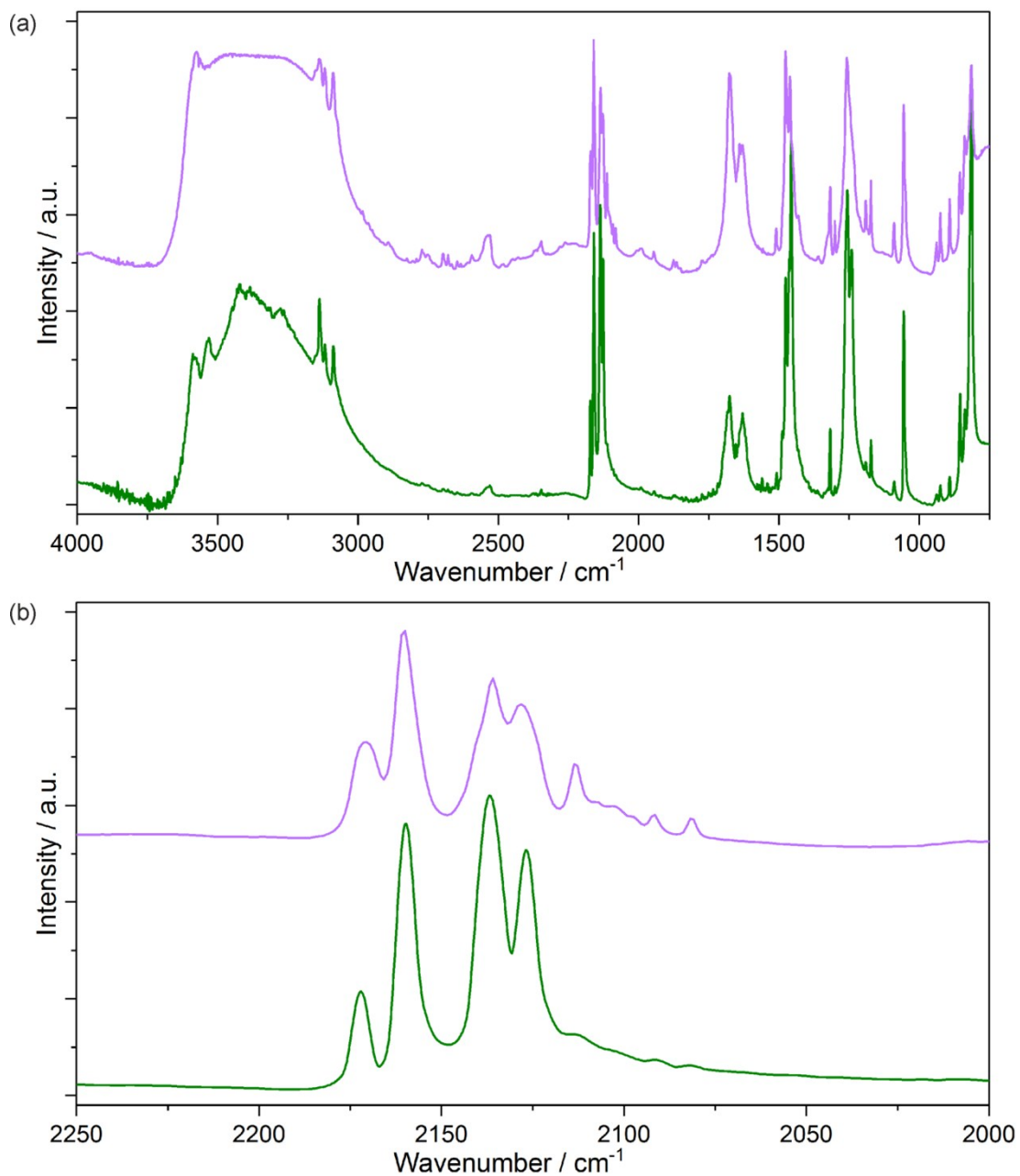


**Figure S1.** Infrared absorption spectrum of the selected single crystal (violet line), and the polycrystalline sample in KBr pellet (green line) of **1** presented in the full 4000–750 cm<sup>-1</sup> measurement range (a), and limited to the 2250–2000 cm<sup>-1</sup> range assigned to the stretching vibrations of cyanides (b).

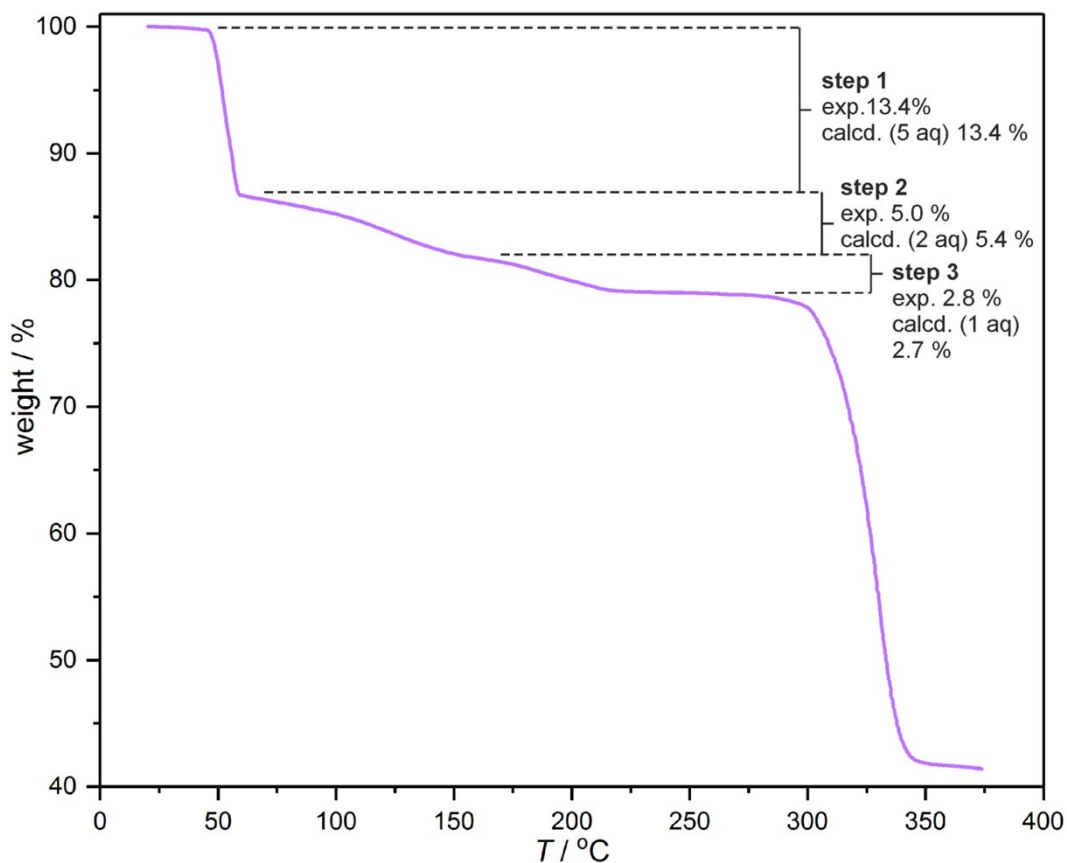


**Figure S2.** Thermogravimetric curve of **1** measured under an air atmosphere with the heating rate of  $1\text{ }^{\circ}\text{C min}^{-1}$  in the 20–375  $^{\circ}\text{C}$  temperature range, with the three indicated steps related to loss of water molecules (see below).

#### Comment to Figure S2:

The polycrystalline sample of **1** with the composition  $\{\text{Nd}^{\text{III}}(\text{pzdo})(\text{H}_2\text{O})_4\}[\text{Co}^{\text{III}}(\text{CN})_6] \cdot 0.5(\text{pzdo}) \cdot 4\text{H}_2\text{O}$  is thermally stable on heating from room temperature to 46 $^{\circ}\text{C}$ . The further heating leads to the rapid decrease of the mass of **1** from 100% to 86.6% (weight loss of 13.4%, **step 1**) in the relatively narrow temperature range of 46–60 $^{\circ}\text{C}$ . This weight loss corresponds to the removal of five water molecules per  $\{\text{Nd}^{\text{III}}\text{Co}^{\text{III}}\}$  unit (calculated weight loss of 13.4%), presumably four hydrogen-bonded and one coordinated water molecules. Thus, at 60 $^{\circ}\text{C}$  the partially dehydrated phase with the composition  $\{\text{Nd}^{\text{III}}(\text{pzdo})(\text{H}_2\text{O})_3\}[\text{Co}^{\text{III}}(\text{CN})_6] \cdot 0.5(\text{pzdo})$  may be postulated. Upon further heating, the mass of **1** slowly decreases in the broad 60–220 $^{\circ}\text{C}$  range reaching the broad plateau in the 220–300 $^{\circ}\text{C}$  region. The gradual decrease of the mass in the 60–220 $^{\circ}\text{C}$  range can be divided into two distinguishable steps. **Step 2** (60–160 $^{\circ}\text{C}$ ) is related to the weight loss of 5.0% which can be ascribed to the removal of two coordinated water molecules (calculated weight loss of 5.4%), while **step 3** (165–220 $^{\circ}\text{C}$ ) with the weight loss of 2.8% can be explained by the removal of the last water molecule, which results in the anhydrous phase with the composition of  $\{\text{Nd}^{\text{III}}(\text{pzdo})_{1.5}[\text{Co}^{\text{III}}(\text{CN})_6]\}$ . The analogous, thermally dehydrated phases have been lately observed in the similar  $\text{Ln}^{\text{III}}(\text{L})\text{--}[\text{Co}^{\text{III}}(\text{CN})_6]^{3-}$  ( $\text{Ln} = \text{Eu, Tb, Dy, Yb}$ ;  $\text{L} = 3\text{-pyridone, 4-pyridone}$ ) coordination systems.<sup>S4-S5, S12-S13</sup> The heating of the sample above 300 $^{\circ}\text{C}$  leads to the dramatic decrease of the mass to 42% remaining at 340 $^{\circ}\text{C}$  which is presumably related to the removal of cyanides and pzdo, and the accompanying decomposition of the material.

**Table S1.** Crystal data and structure refinement for **1**

Compound		<b>1</b>
method		single-crystal XRD
formula		Nd <sub>1</sub> Co <sub>1</sub> C <sub>12</sub> H <sub>22</sub> N <sub>9</sub> O <sub>11</sub>
formula weight [g·mol <sup>-1</sup> ]		671.55
<i>T</i> [K]		120(2)
$\lambda$ [Å]		0.71073 (Mo K $\alpha$ )
crystal system		triclinic
space group		<i>P</i> $\bar{1}$
unit cell	<i>a</i> [Å]	8.5982(2)
	<i>b</i> [Å]	10.1946(2)
	<i>c</i> [Å]	14.0611(4)
	$\alpha$ [deg]	76.1670(10)
	$\beta$ [deg]	75.0010(10)
	$\gamma$ [deg]	90.050(2)
<i>V</i> [Å <sup>3</sup> ]		1153.42(5)
<i>Z</i>		2
calculated density [g·cm <sup>-3</sup> ]		1.934
absorption coefficient [cm <sup>-1</sup> ]		3.016
<i>F</i> (000)		664
crystal size [mm × mm × mm]		0.04 × 0.08 × 0.16
$\theta$ range [deg]		2.251–25.051
limiting indices		-10 < <i>h</i> < 10 -12 < <i>k</i> < 12 -16 < <i>l</i> < 16
collected reflections		17373
unique reflections		4073
<i>R</i> <sub>int</sub>		0.0461
completeness [%]		99.8
max. and min. transmission		0.644 and 0.889
refinement method		full-matrix least-squares on <i>F</i> <sup>2</sup>
data/restraints/parameters		4073/18/395
GOF on <i>F</i> <sup>2</sup>		1.191
final <i>R</i> indices		<i>R</i> <sub>1</sub> = 0.0237 [ <i>I</i> > 2 $\sigma$ ( <i>I</i> )] <i>wR</i> <sub>2</sub> = 0.0784 (all data)
largest diff peak and hole		0.798 and -0.878 e <sup>-</sup> ·Å <sup>-3</sup>

**Table S2.** Detailed structure parameters of **1**

Details of [Nd <sup>III</sup> (pzdo)(H <sub>2</sub> O) <sub>4</sub> (NC) <sub>3</sub> ] complex		Details of [Co <sup>III</sup> (CN) <sub>6</sub> ] <sup>3-</sup> complex	
Parameter	Value [Å, °]	Parameter	Value [Å, °]
Nd1–N1	2.593(4)	Co1–C1	1.890(5)
Nd1–N5	2.591(4)	Co1–C2	1.902(5)
Nd1–N6	2.596(4)	Co1–C3	1.883(5)
Nd1–O1	2.486(3)	Co1–C4	1.893(5)
Nd1–O2	2.530(3)	Co1–C5	1.889(5)
Nd1–O3	2.504(3)	Co1–C6	1.891(5)
Nd1–O4	2.535(3)	C1–N1	1.149(6)
Nd1–O5	2.463(3)	C2–N2	1.148(6)
Nd1–O6	2.477(3)	C3–N3	1.159(6)
Nd1–N1–C1	177.4(3)	C4–N4	1.150(6)
Nd1–N5–C5	170.8(4)	C5–N5	1.149(6)
Nd1–N6–C6	146.6(4)	C6–N6	1.146(6)
N1–Nd1–N5	106.46(12)	Co1–C1–N1	176.9(4)
N1–Nd1–N6	69.88(12)	Co1–C2–N2	179.8(4)
N5–Nd1–N6	69.79(12)	Co1–C3–N3	178.7(4)
Nd1–O5–N7 (pzdo)	130.9(3)	Co1–C4–N4	175.5(4)
Nd1–O6–N8 (pzdo)	129.9(3)	Co1–C5–N5	177.9(4)
O5–Nd1–O6 (pzdo)	82.42(10)	Co1–C6–N6	178.3(4)
Nd1–(pzdo)–Nd1'	8.598	Co1–(C1N1)–Nd1	5.628
Nd1–([Co(CN) <sub>6</sub> ])–Nd1'	8.439	Co1–(C2N2)–Nd1	5.606
Nd1–O7(pzdo)	4.619	Co1–(C5N5)–Nd1	5.382

**Table S3.** Results of Continuous Shape Measure Analysis for the nine-coordinated  $[\text{Nd}^{\text{III}}(\text{pzdo})(\text{H}_2\text{O})_4(\text{NC})_3]$  complex in **1**

Nd complex	CSM parameters				Geometry
	HBPY-9 ( $D_{7h}$ )	CCU-9 ( $C_{4v}$ )	CSAPR-9 ( $C_{4v}$ )	TCTPR-9 ( $D_{3h}$ )	
$[\text{Nd}^{\text{III}}(\text{pzdo})(\text{H}_2\text{O})_4(\text{NC})_3]$ { $\text{N}_3\text{O}_6$ } coordination sphere	19.291	9.867	0.325	0.996	CSAPR-9

\* CSM parameters:

CSM HBPY-9 = the parameter related to the heptagonal bipyramid ( $D_{7h}$  symmetry)

CSM CCU-9 = the parameter related to the spherical-relaxed capped cube ( $C_{4v}$  symmetry)

CSM CSAPR-9 = the parameter related to the capped square antiprism ( $C_{4v}$  symmetry)

CSM TCTPR-9 = the parameter related to the tricapped trigonal prism ( $D_{3h}$  symmetry)

CSM = 0 for the ideal geometry and the increase of CSM parameter corresponds to the increasing distortion from the ideal polyhedron.<sup>S10-S11</sup>

**Table S4.** Results of Continuous Shape Measure Analysis for the six-coordinated  $[\text{Co}^{\text{III}}(\text{CN})_6]^{3-}$  complex in **1**

Co complex	CSM parameters				Geometry
	HP-6 ( $D_{6h}$ )	PPY-6 ( $C_{5v}$ )	OC-6 ( $O_h$ )	TPR-6 ( $D_{3h}$ )	
$[\text{Co}^{\text{III}}(\text{CN})_6]^{3-}$ { $\text{N}_6$ } coordination sphere	32.336	28.996	0.039	15.799	OC-6

\* CSM parameters:

CSM HP-6 = the parameter related to the hexagon ( $D_{6h}$  symmetry)

CSM PPY-6 = the parameter related to the pentagonal pyramid ( $C_{5v}$  symmetry)

CSM OC-6 = the parameter related to the octahedron ( $O_h$  symmetry)

CSM TPR-6 = the parameter related to the trigonal prism ( $D_{3h}$  symmetry)

CSM = 0 for the ideal geometry and the increase of CSM parameter corresponds to the increasing distortion from the ideal polyhedron.<sup>S10-S11</sup>

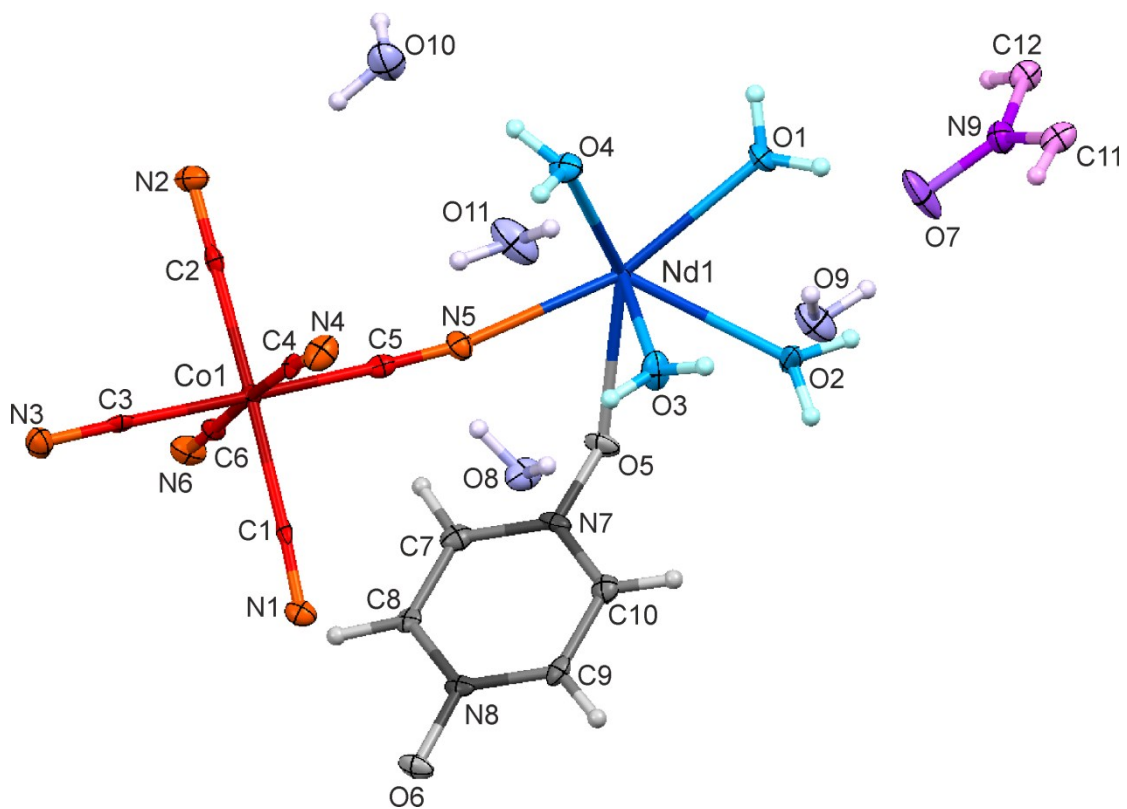


**Figure S3.** Asymmetric unit of **1** with the non-hydrogen atoms labelling scheme. Atoms are shown with 50% probability level. The hydrogen atoms were drawn as fixed-size spheres of 0.13 Å radius.

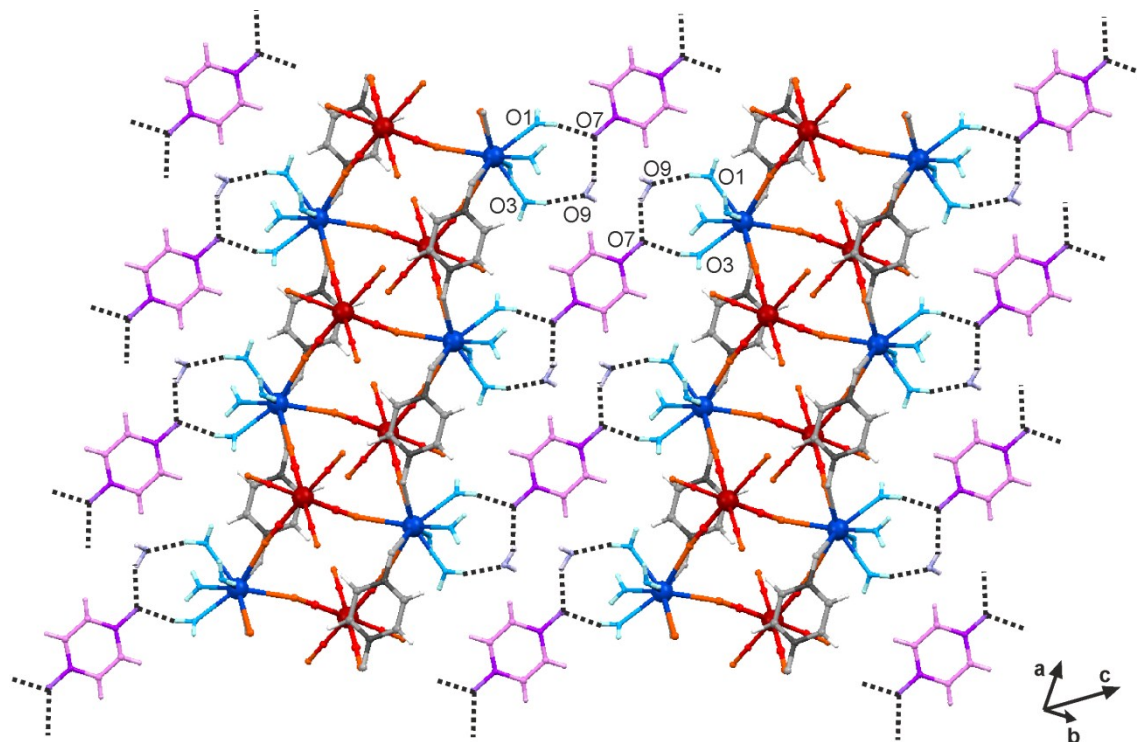


**Figure S4.** The supramolecular arrangement of cyanido-bridged chains and non-coordinated pzdo molecules of **1** with the insight into the related hydrogen bonds. The dotted lines represent the hydrogen bonds. The respective interatomic distances of the hydrogen bonds are collected in Table S5.

**Table S5.** Detailed interatomic distances of hydrogen bonds network of **1**.

Hydrogen bonds	Value, [Å]
Hydrogen bonds related to the alignment of non-coordinated pzdo molecules (Figure S4)	
O7 (pzdo) - (H1A) - O1	2.68
O7 (pzdo) - (H9B) - O9	2.71
O9 - (H3B) - O3	2.69
Other interchain hydrogen bonds involving non-coordinated water molecules	
O1 - (H1B) - O8	2.81
O2 - (H2A) - N2 (CN)	2.94
O2 - (H2B) - N3 (CN)	2.86
O3 - (H3A) - O8	2.90
O4 - (H4A) - O11	2.72
O4 - (H4B) - O10	2.79
O8 - (H8A) - N4 (CN)	3.29
O8 - (H8B) - N4 (CN)	2.87
O8 - (H8B) - O11	3.15
O9 - (H9A) - O10	2.85
O11 - (H11A) - N4 (CN)	3.02
O11 - (H11B) - O4	2.88

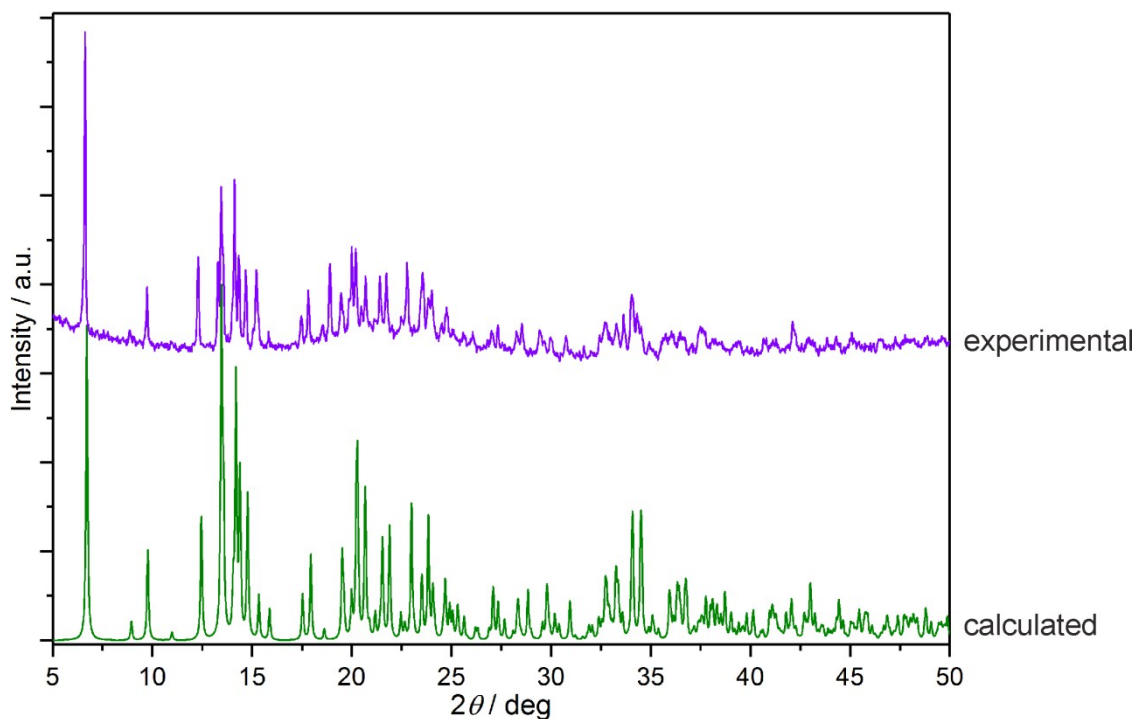


**Figure S5.** Experimental powder diffraction pattern of the polycrystalline sample of **1** (violet) compared with the respective PXRD pattern calculated from the structural model obtained from the single crystal X-ray structural analysis (green). Only the representative range of 5–50° of  $2\theta$  angle is presented for clarity. The consequent small shift of all peaks between the experimental, and the calculated patterns is due to the standard temperature effect, as the PXRD experiment was conducted at room temperature while the single crystal X-ray measurement was executed at low temperature of 120(2) K.

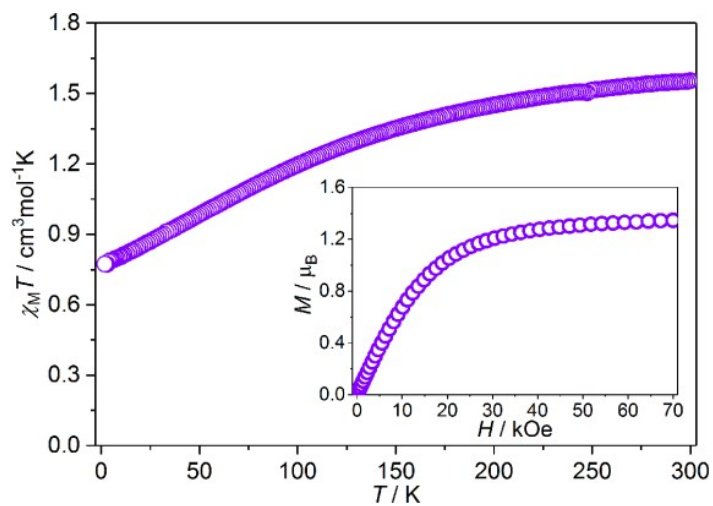


**Figure S6.** Direct-current (*dc*) magnetic properties of **1**: temperature dependence of the magnetic susceptibility–temperature,  $\chi_M T$  product at  $H_{dc} = 1 \text{ kOe}$ , and field dependence of magnetization,  $M$  at  $T = 1.8 \text{ K}$  (the inset).

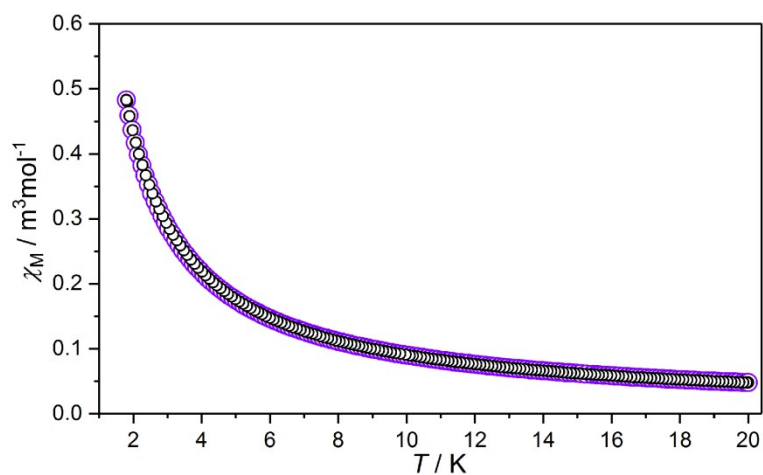


**Figure S7.** Zero-field cooled (ZFC, violet points) and field-cooled (FC, black points) magnetic susceptibility curves of **1** under an external *dc* magnetic field of 15 Oe in the 1.8–20 K range.

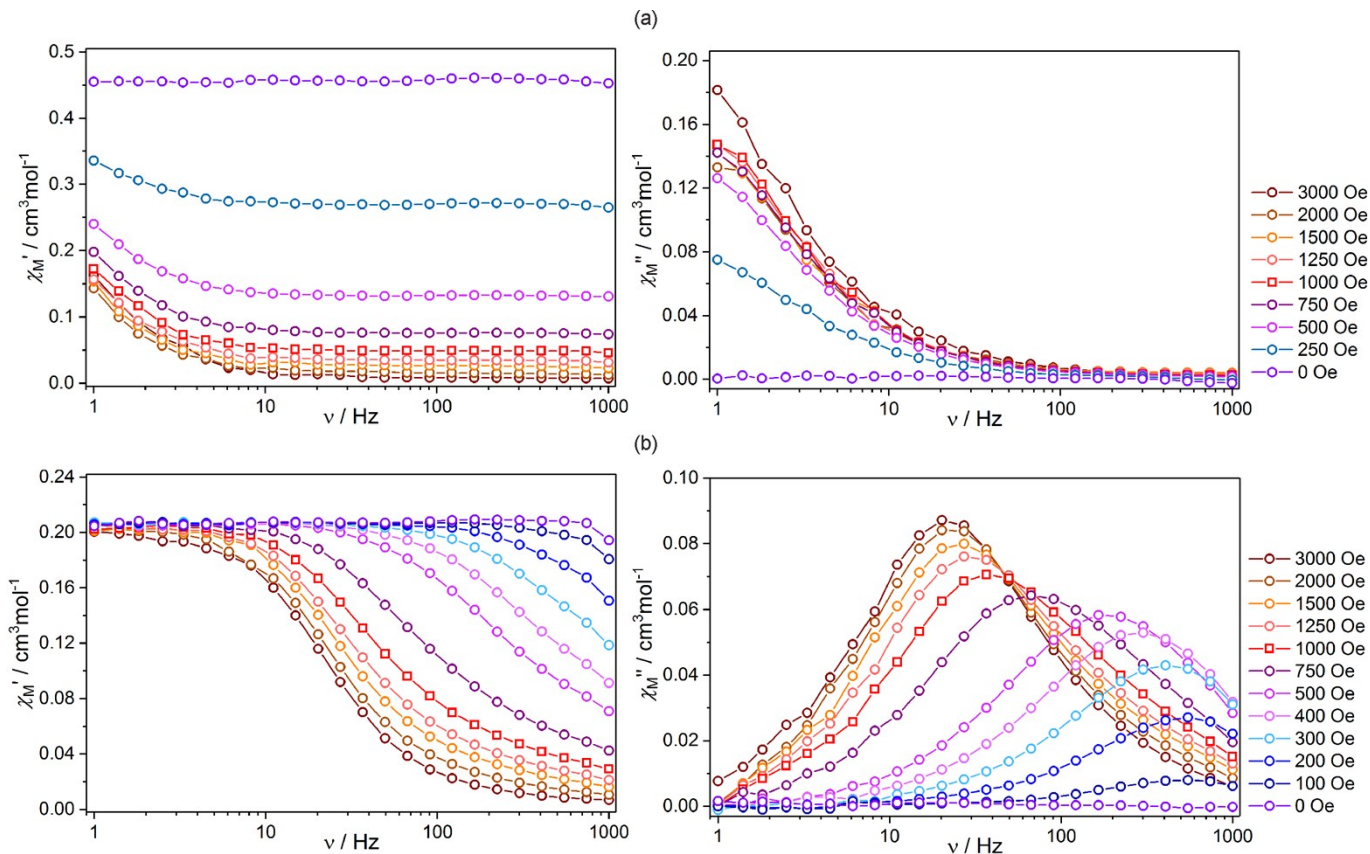


**Figure S8.** Frequency dependences of in-phase  $\chi_M'$  (left) and out-of-phase  $\chi_M''$  (right) magnetic susceptibilities of **1** under *ac* magnetic field of 1 Oe, at  $T = 1.8$  K (a) and  $T = 4$  K (b), at indicated values of *dc* magnetic field. Solid lines are added only to guide the eye. The data for the *dc* magnetic field of 1000 Oe, selected for detailed *ac* magnetic studies, was distinguished by red square points.

**Table S6.** Parameters obtained by fitting the Argand  $\chi_M''-\chi_M'$  plots ( $H_{dc} = 1000$  Oe, Figure 4) of **1** using the generalized Debye model.

$T / \text{K}$	$\chi_S$ $\text{cm}^3\text{mol}^{-1}$	$\chi_T$ $\text{cm}^3\text{mol}^{-1}$	$\tau / \text{s}$	$\alpha$
1.8	0.0501	0.455	<b>0.262</b>	0.118
2.0	0.0446	0.409	<b>0.164</b>	0.105
2.2	0.0405	0.367	<b>0.0908</b>	0.096
2.4	0.0371	0.338	<b>0.0526</b>	0.125
2.6	0.0337	0.316	<b>0.0332</b>	0.173
2.8	0.0301	0.298	<b>0.0230</b>	0.221
3.0	0.0295	0.280	<b>0.0166</b>	0.233
3.2	0.0284	0.266	<b>0.0124</b>	0.249
3.4	0.0293	0.249	<b>0.00904</b>	0.227
3.6	0.0296	0.236	<b>0.00666</b>	0.212
3.8	0.0292	0.222	<b>0.00479</b>	0.187
4.0	0.0287	0.211	<b>0.00345</b>	0.162
4.2	0.0290	0.199	<b>0.00240</b>	0.124
4.4	0.0281	0.191	<b>0.00170</b>	0.104
4.6	0.0272	0.182	<b>0.00121</b>	0.082
4.8	0.0273	0.174	<b>0.000853</b>	0.056
5.0	0.0279	0.167	<b>0.000617</b>	0.035
5.2	0.0284	0.160	<b>0.000453</b>	0.018
5.4	0.0276	0.155	<b>0.000334</b>	0.017
5.6	0.0277	0.149	<b>0.000248</b>	0.018
5.8	0.0278	0.145	<b>0.000186</b>	0.018
6.0	0.0288	0.140	<b>0.000142</b>	0.019
6.2	0.0332	0.136	<b>0.000115</b>	0.020

The following equations representing the generalized Debye model for a single relaxation process were used:

$$\chi'(\omega) = \chi_S + (\chi_T - \chi_S) \frac{1 + (\omega\tau)^{1-\alpha} \sin\left(\frac{\pi\alpha}{2}\right)}{1 + 2(\omega\tau)^{1-\alpha} \sin\left(\frac{\pi\alpha}{2}\right) + (\omega\tau)^{2(1-\alpha)}}$$

$$\chi''(\omega) = (\chi_T - \chi_S) \frac{(\omega\tau)^{1-\alpha} \cos\left(\frac{\pi\alpha}{2}\right)}{1 + 2(\omega\tau)^{1-\alpha} \sin\left(\frac{\pi\alpha}{2}\right) + (\omega\tau)^{2(1-\alpha)}}$$

where

$\chi_S$  = the adiabatic susceptibility (at infinitely high frequency of  $ac$  field),

$\chi_T$  = the isothermal susceptibility (at infinitely low frequency of  $ac$  field),

$\tau$  = the relaxation time,

$\alpha$  = the distribution (Cole-Cole) parameter,

and  $\omega = 2\pi\nu$ , with  $\nu$  being the frequency in [Hz] units.<sup>S14-S15</sup>

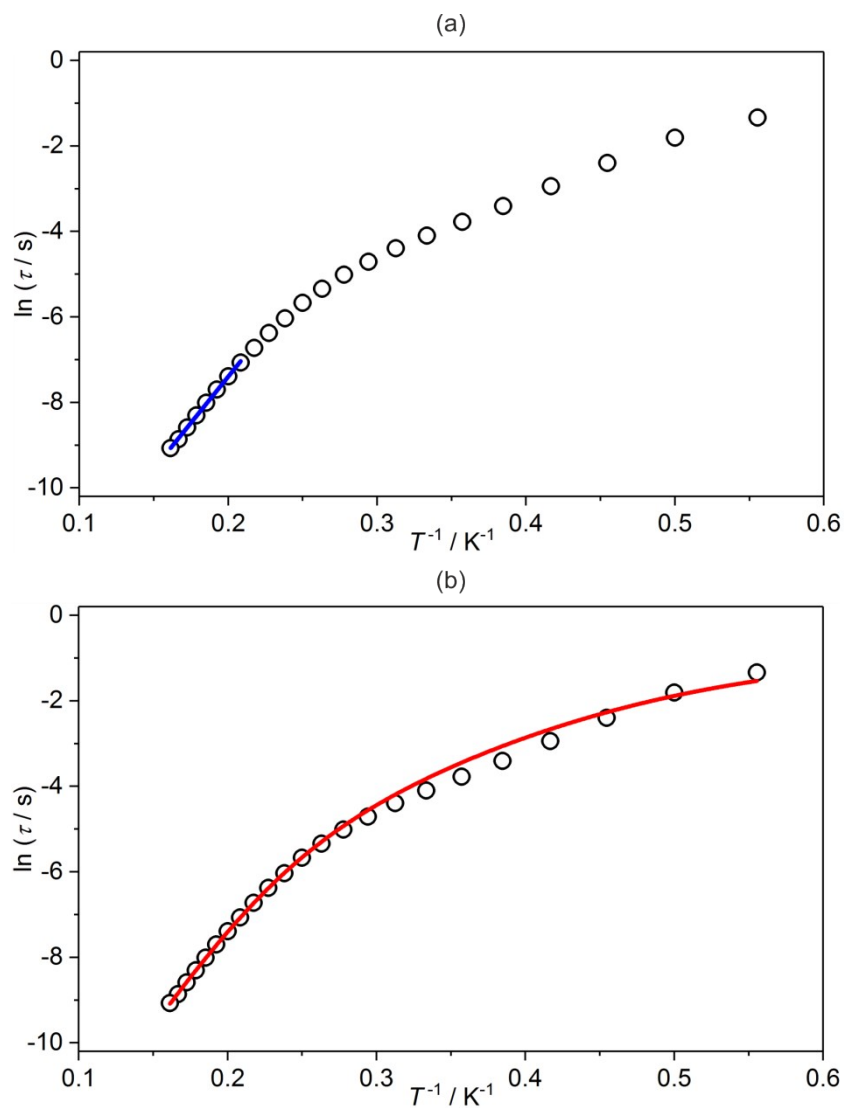


**Figure S9.** Temperature dependence of the relaxation time ( $\tau$ ) of **1** in the form of  $\ln(\tau)$  versus  $T^{-1}$  plot for  $H_{ac} = 1$  Oe,  $H_{dc} = 1000$  Oe with the linear fitting for the limited temperature range of 4.8–6.2 K, according to the Arrhenius law (a), and the non-linear fitting taking into account the Orbach and Raman relaxation processes, and the quantum tunnelling of magnetization effect in the broader 1.8–6.2 K range (b). See the main text for details.

**Table S7.** Overview of Nd<sup>III</sup> complexes revealing Single-Molecule Magnet behaviour.

Compound	$\Delta E/k_B / K$	$\tau_0 / s$	$H_{dc} / Oe$	Ref.
<b>1</b>	51(2)	$4.5(9) \cdot 10^{-8}$	1000	this work
zero-dimensional molecular systems				
[Li(dme) <sub>3</sub> ][Nd <sup>III</sup> (COT <sup>''</sup> ) <sub>2</sub> ] (dme = dimethoxyethane; COT <sup>''</sup> = bis(trimethylsilyl)cyclooctatetraenyl dianion)	21	$5.5 \cdot 10^{-5}$	1000	S16
[Nd <sup>III</sup> (Tp) <sub>3</sub> ] (Tp = trispyrazolylborate)	4.1(1)	$4.2(2) \cdot 10^{-5}$	100	S17
[Nd <sup>III</sup> ( <sup>t</sup> BuPO(NH <sup>i</sup> Pr) <sub>2</sub> ) <sub>2</sub> (H <sub>2</sub> O) <sub>5</sub> ] <sub>3</sub> ·H <sub>2</sub> O	24.69	$5.03 \cdot 10^{-6}$	0	S18
	16.08	$2.64 \cdot 10^{-4}$	0	
	39.21	$8.98 \cdot 10^{-7}$	2000	
Na <sub>9</sub> [Nd <sup>III</sup> (W <sub>5</sub> O <sub>18</sub> ) <sub>2</sub> ]	73.9	$3.55 \cdot 10^{-10}$	1000	S19
[Nd <sup>III</sup> (NO <sub>3</sub> ) <sub>3</sub> (18-crown-6)]	33.4(5)	$1.6(2) \cdot 10^{-9}$	1000	S20
[Nd <sup>III</sup> (NO <sub>3</sub> ) <sub>3</sub> (1,10-diaza-18-crown-6)]	73(2)	$1.4(6) \cdot 10^{-10}$	1000	S20
(NH <sub>2</sub> Me <sub>2</sub> ) <sub>3</sub> {[Nd <sup>III</sup> (Mo <sub>4</sub> O <sub>13</sub> )(dmf) <sub>4</sub> ] <sub>3</sub> (btc) <sub>2</sub> }·8(dmf) (btc = 1,3,5-benzentricarboxylate anion)	34.06	$4.69 \cdot 10^{-8}$	500	S21
[Nd <sup>III</sup> (Cp <sup>*</sup> ) <sub>2</sub> ](BPh <sub>4</sub> ) (Cp <sup>*</sup> = pentamethylcyclopentadienyl anion)	41(2)	$1.4(4) \cdot 10^{-6}$	1000	S22
one-dimensional coordination polymers				
[Nd <sup>III</sup> <sub>2</sub> (CNCH <sub>2</sub> COO) <sub>6</sub> (H <sub>2</sub> O) <sub>4</sub> ] <sub>2</sub> ·2H <sub>2</sub> O	26.6(1)	$1.75 \cdot 10^{-7}$	1500	S23
[Nd <sup>III</sup> (3,5-dnb) <sub>3</sub> (H <sub>2</sub> O) <sub>2</sub> ]·MeCN (3,5-dnb = 3,5-dinitrobenzoic acid anion)	27 K	$4.1 \cdot 10^{-7}$	2000	S24
[Nd <sup>III</sup> (2,4-dnb) <sub>2</sub> (CH <sub>3</sub> COO)(H <sub>2</sub> O) <sub>2</sub> ] (2,4-dnb = 2,4-dinitrobenzoic acid anion)	29 K	$3.1 \cdot 10^{-7}$	3500	S24

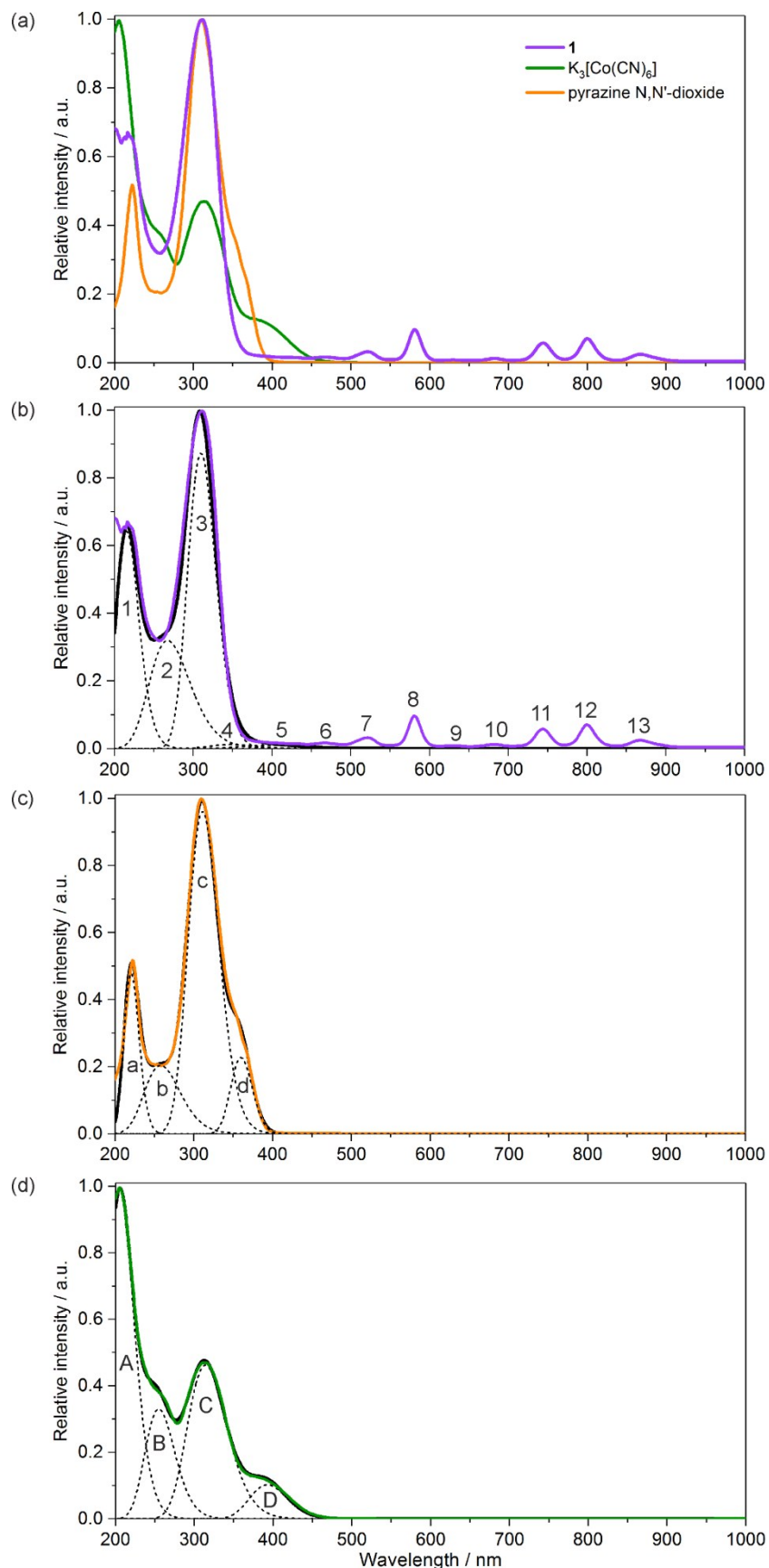


**Figure S10.** Solid state UV-Vis-NIR absorption (Kubelka-Munk function) spectra of **1** (a-b) compared with the relevant spectra of pyrazine  $N,N'$ -dioxide (c) and  $K_3[Co(CN)_6]$  (d). The coloured solid lines correspond to the experimental data, the dotted lines show the components of the UV-Vis bands below 450 nm (Table S8), and the solid black lines are the calculates sums.

**Table S8.** Analysis of the solid state UV-Vis-NIR absorption spectrum of **1** compared with the analyses of the relevant spectra of pyrazine N,N'-dioxide (pzdo) and  $K_3[Co^{III}(CN)_6]$  (see Figure S9).

compound (figure)	peak no.	$\lambda_{max}$ [nm]	intensity of maximum [a.u.]	interpretation
<b>1</b> (figure S9b)	1	215	0.64	combined contributions from singlet to singlet transitions ( $\pi \rightarrow \pi^*$ ) of pzdo and d-d transition of $Co^{III-L.S.}: {}^1A_{1g} \rightarrow {}^1E_g$
	2	265	0.32	combined contributions from singlet to singlet transitions ( $\pi \rightarrow \pi^*$ ) of pzdo and d-d transition of $Co^{III-L.S.}: {}^1A_{1g} \rightarrow {}^1T_{2g}$
	3	310	0.87	combined contributions from singlet to singlet transitions ( $\pi \rightarrow \pi^*$ ) of pzdo and d-d transition of $Co^{III-L.S.}: {}^1A_{1g} \rightarrow {}^1T_{1g}$
	4	353	0.01	singlet to singlet transitions of pzdo (overlapping $n \rightarrow \pi^*$ and $\pi \rightarrow \pi^*$ bands)
	5	401	0.01	d-d transition of $Co^{III-L.S.}: {}^1A_{1g} \rightarrow {}^3T_{1g}$
	6	467	0.02	f-f transition of $Nd^{III}: S_{25-S_{26}} {}^4I_{9/2} \rightarrow {}^2G_{9/2}, {}^4G_{11/2}, {}^2K_{15/2}$
	7	521	0.03	f-f transition of $Nd^{III}: {}^4I_{9/2} \rightarrow {}^4G_{7/2}, {}^4G_{9/2}, {}^2K_{13/2}$
	8	581	0.10	f-f transition of $Nd^{III}: {}^4I_{9/2} \rightarrow {}^2G_{7/2}, {}^4G_{5/2}$
	9	631	0.01	f-f transition of $Nd^{III}: {}^4I_{9/2} \rightarrow {}^2H_{11/2}$
	10	682	0.01	f-f transition of $Nd^{III}: {}^4I_{9/2} \rightarrow {}^4F_{9/2}$
	11	743	0.06	f-f transition of $Nd^{III}: {}^4I_{9/2} \rightarrow {}^4S_{3/2}, {}^4F_{7/2}$
	12	799	0.07	f-f transition of $Nd^{III}: {}^4I_{9/2} \rightarrow {}^2H_{9/2}, {}^4F_{5/2}$
	13	868	0.03	f-f transition of $Nd^{III}: {}^4I_{9/2} \rightarrow {}^4F_{3/2}$
pzdo (figure S9c)	a	220	0.48	singlet to singlet transitions ( $\pi \rightarrow \pi^*$ ) <sup>S27-S28</sup>
	b	258	0.21	
	c	311	0.96	
	d	360	0.23	singlet to singlet transitions (overlapping $n \rightarrow \pi^*$ and $\pi \rightarrow \pi^*$ bands) <sup>S27-S28</sup>
$K_3[Co(CN)_6]$ (figure S9d)	A	205	0.99	d-d transition of $Co^{III-L.S.}: S_{29-S_{31}} {}^1A_{1g} \rightarrow {}^1E_g$
	B	255	0.33	d-d transition of $Co^{III-L.S.}: {}^1A_{1g} \rightarrow {}^1T_{2g}$ (minor contribution of ${}^1A_{1g} \rightarrow {}^5T_{2g}$ )
	C	314	0.46	d-d transition of $Co^{III-L.S.}: {}^1A_{1g} \rightarrow {}^1T_{1g}$ (minor contribution of ${}^1A_{1g} \rightarrow {}^3T_{2g}$ )
	D	393	0.10	d-d transition of $Co^{III-L.S.}: {}^1A_{1g} \rightarrow {}^3T_{1g}$

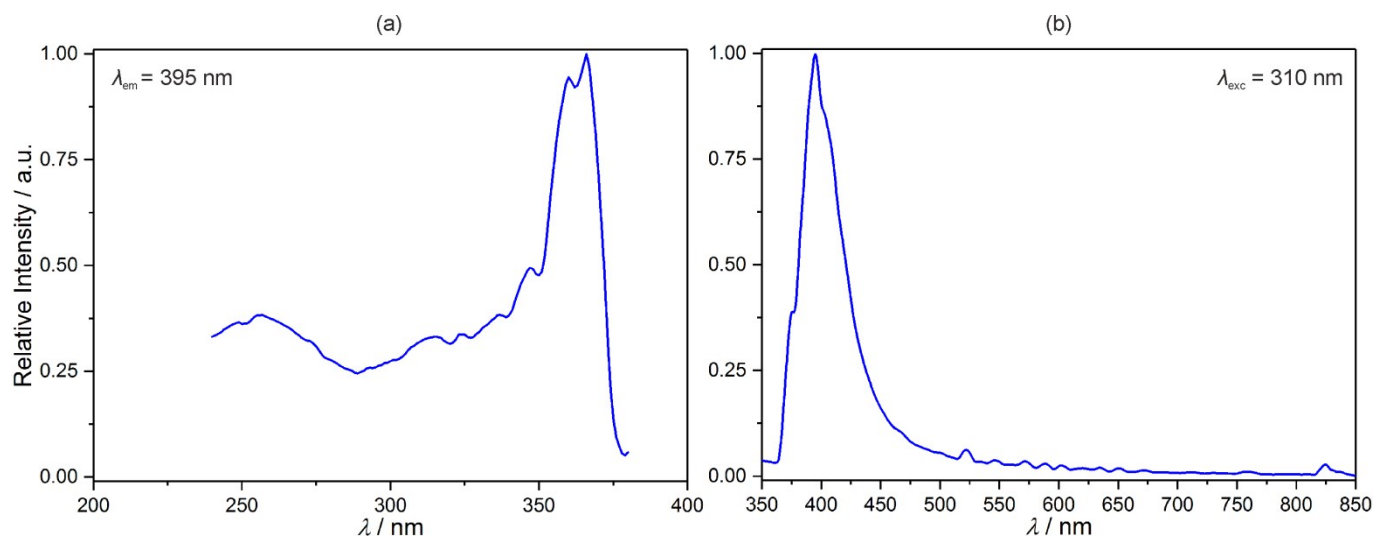


**Figure S11.** Solid state excitation (a) and emission (b) spectra of pyrazine N,N'-dioxide collected at liquid nitrogen temperature of 77 K.

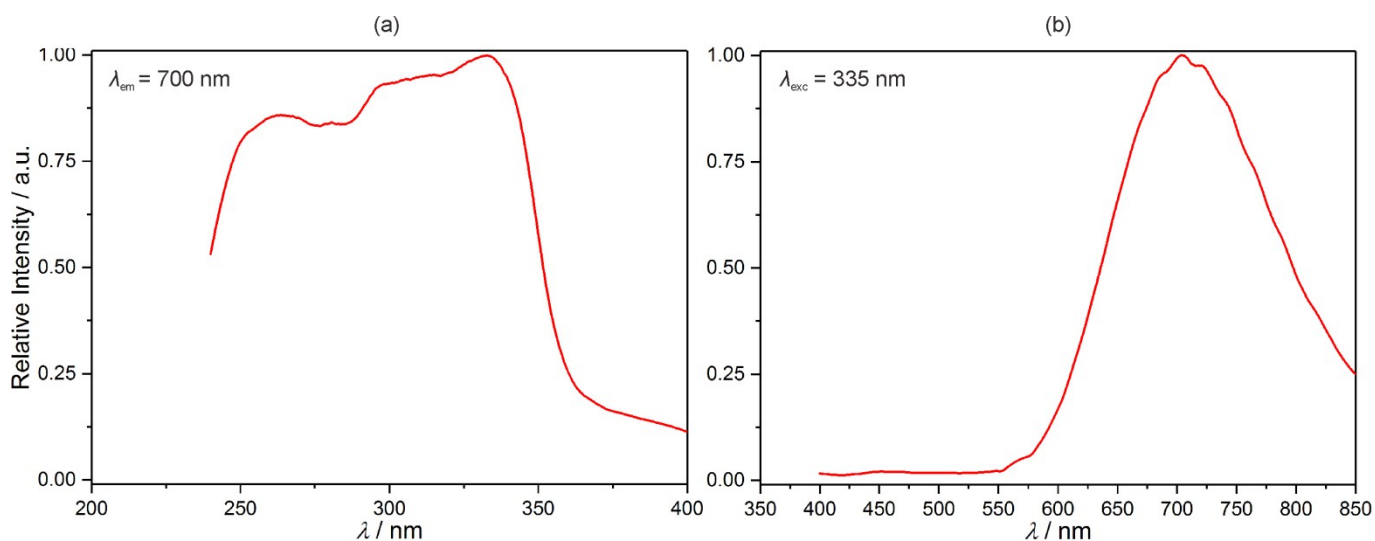


**Figure S12.** Solid state excitation (a) and emission (b) spectra of  $K_3[Co^{III}(CN)_6]$  collected at liquid nitrogen temperature of 77 K.

## References to Supporting Information

- [S1] R. Podgajny, D. Pinkowicz, T. Korzeniak, W. Nitek, M. Rams and B. Sieklucka, *Inorg. Chem.*, 2007, **46**, 10416.
- [S2] W.-T. Chang, G.-C. Guo, M.-S. Wang, G. Xu, L.-Z. Cai, T. Akitsu, M. Akita-Tanaka, A. Matsuchita and J.-S. Huang, *Inorg. Chem.*, 2007, **46**, 2105.
- [S3] Y. Zhang, Z. Guo, S. Xie, H.-L. Li, W.-H. Zhu, L. Liu, X.-Q. Dong, W.-X. Ren, L.-Z. Liu and A. K. Powell, *Inorg. Chem.*, 2015, **54**, 10316.
- [S4] S. Chorazy, M. Rams, K. Nakabayashi, B. Sieklucka and S. Ohkoshi, *Chem. Eur. J.*, 2016, **22**, 7371.
- [S5] S. Chorazy, M. Rams, J. Wang, B. Sieklucka and S. Ohkoshi, *Dalton Trans.*, 2017, **46**, 13668.
- [S6] G. Sheldrick, *Acta Crystallogr., Sect. A: Found Crystallogr.*, 2008, **64**, 112.
- [S7] G. Sheldrick, *Acta Crystallogr., Sect. C: Struct. Chem.*, 2015, **71**, 3.
- [S8] L. Farrugia, *J. Appl. Crystallogr.*, 2012, **45**, 849.
- [S9] G. A. Bain and J. F. Berry, *J. Chem. Educ.*, 2008, **85**, 532.
- [S10] M. Llunell, D. Casanova, J. Cirera, J. Bofill, P. Alemany, S. Alvarez, M. Pinsky, D. Avnir, *SHAPE v. 2.1. Program for the Calculation of Continuous Shape Measures of Polygonal and Polyhedral Molecular Fragments*, University of Barcelona: Barcelona, Spain, 2013.
- [S11] D. Casanova, J. Cirera, M. Llunell, P. Alemany, D. Avnir and S. Alvarez, *J. Am. Chem. Soc.*, 2004, **126**, 1755.
- [S12] S. Chorazy, J. Wang and S. Ohkoshi, *Dalton Trans.*, 2016, **52**, 10795.
- [S13] S. Chorazy, K. Kumar, K. Nakabayashi, B. Sieklucka and S. Ohkoshi, *Inorg. Chem.*, 2017, **56**, 5239.
- [S14] Y.-N. Guo, G.-F. Xu, Y. Guo and J. Tang, *Dalton Trans.*, 2011, **40**, 9953.
- [S15] M. Ramos Silva, P. Martin-Ramos, J. T. Coutinho, L. C. J. Perreira and J. Martin-Gil, *Dalton Trans.*, 2014, **43**, 6752.
- [S16] J. J. Le Roy, S. I. Gorelsky, I. Korobkov and M. Murugesu, *Organometallics*, 2015, **34**, 1415.
- [S17] J. D. Rinehart and J. R. Long, *Dalton Trans.*, 2012, **41**, 13572.
- [S18] S. K. Gupta, T. Rajeshkumar, G. Rajaraman and R. Murugavel, *Chem. Commun.*, 2016, **52**, 7168.
- [S19] J. J. Baldovi, J. M. Clemente-Juan, E. Coronado, Y. Duan, A. Gaita-Arino and C. Gimenez-Saiz, *Inorg. Chem.*, 2014, **53**, 9976.
- [S20] H. Wada, S. Ooka, T. Yamamura and T. Kajiwara, *Inorg. Chem.*, 2017, **56**, 147.
- [S21] H. Zhang, X. Wu, J. Liao, X. Kuang, W. Yang and C. Lu, *Dalton Trans.*, 2018, doi: 10.1039/C7DT04908K.
- [S22] S. Demir, K. R. Meihaus and J. R. Long, *J. Organomet. Chem.*, 2017, doi.org/10.1016/j.jorganchem.2017.10.035.
- [S23] A. Arauzo, A. Lazarescu, S. Shova, E. Bartolome, R. Cases, J. Luzon, J. Bartolome and C. Turta, *Dalton Trans.*, 2014, **43**, 12342.

- [S24] A. K. Jassal, N. Aliaga-Alcalde, M. Corbella, D. Aravena, E. Ruiz and G. Hundal, *Dalton Trans.*, 2015, **44**, 15774.
- [S25] S. P. Sinha, *Spectrochem. Acta*, 1966, **22**, 57.
- [S26] B. Chen, J. Xu, N. Dong, H. Liang, Q. Zhang and M. Yin, *Spectrochem. Acta A*, 2004, **60**, 3113.
- [S27] J. Del Bene and H. H. Jaffe, *J. Chem. Physics*, 1968, **49**, 1221.
- [S28] M. Yamakawa, T. Kubota and H. Akazawa, *Theoret. Chim Acta*, 1969, **15**, 244.
- [S29] V. M. Miskowski, H. B. Gray, R. B. Wilson and E. I. Solomon, *Inorg. Chem.*, 1979, **18**, 1410.
- [S30] H. Kunkely and A. Vogler, *Inorg. Chem. Commun.*, 2004, **7**, 770.
- [S31] T. Lazarides, G. M. Davies, H. Adams, C. Sabatini, F. Barigelletti, A. Barbieri, S. J. A. Pope, S. Faulkner and M. D. Ward, *Photochem. Photobiol. Sci.*, 2007, **6**, 1152.